

# Quantum Synchronisation Enabled by Dynamical Symmetries and Dissipation

J. Tindall<sup>1</sup>, C. Sánchez Muñoz<sup>1</sup>, B. Buča<sup>1</sup> and D. Jaksch<sup>1,2</sup>

<sup>1</sup>*Clarendon Laboratory, University of Oxford, Parks Road, Oxford OX1 3PU, United Kingdom*

(Dated: December 21, 2024)

In nature, instances of synchronisation abound across a diverse range of environments. In the quantum regime, however, synchronisation is typically observed by identifying an appropriate parameter regime in a specific system. In this work we show that this need not be the case, identifying symmetry-based conditions which, when satisfied, guarantee completely synchronous, entangled limit cycles between the individual constituents of a generic open quantum system - no restrictions are placed on its microscopic details. We describe these systems as possessing a strong dynamical symmetry and we prove that, to first order, they are completely robust to symmetry-breaking perturbations. Using these ideas we identify two central examples where synchronisation arises via this qualitatively new mechanism: a chain of quadratically dephased spin-1s and the many-body charge-dephased Hubbard model. In both cases, due to their dynamical symmetries, perfect phase-locking occurs throughout the system, regardless of the specific microscopic parameters or initial states. Furthermore, when these systems are perturbed, their non-linear responses elicit long-lived signatures of both phase and frequency-locking.

## I. INTRODUCTION

Synchronization is a fascinating and multi-disciplinary topic in modern science, focussed on understanding how a collection of individual bodies adjust their natural rhythms and phases through their interactions with each other and the environment [1–5]. In a striking display of cooperative behaviour, this adjustment can lead to a variety of phenomena such as the ‘winking’ of fireflies, the behavioural synchrony of groups of strangers or the coupling of a pair of pendulums through a mutual support [6–8].

The study of synchronisation in quantum systems has attracted significant attention [9–15]. In this regime, synchronisation takes on a fairly broad definition due to the variety of cooperative, entangled behaviour that can occur [16]. The formation of a Bose-Einstein condensate (BEC), for example, could be considered perfect synchronisation [17] due to the collective condensation of the atoms in the bosonic gas. In closer analogy to classical systems, models of self-sustained quantum oscillators, such as quantum Van der Pol oscillators [18–20] or pairs of micromasers [21], have been shown to lock phases and reach coupled limit cycles. Quantum effects play a decisive role in either enhancing [22, 23] or hindering [24] this synchronicity. Under the mean-field approximation, these results have been extended to larger systems of oscillators where the underlying mechanism for synchronisation is a reduction in the uncertainty in the phase distribution at the expense of the certainty in the number distribution [18].

Recently, there has been a focus on observing synchronisation in the limit cycles of quantum systems which have no classical analogue [9–11]. The qutrit has been proposed as a logical candidate for this and recent work has demonstrated that it can be entrained to an external signal [9, 11] or phase-locked and entangled with a second spin [10]. In these single or two qutrit systems, synchronisation emerges due to careful control over the

Hamiltonian and dissipation parameters and is witnessed through both the phase space portrait and entanglement profile of the spins.

One of the most remarkable features of synchronisation in the classical regime, however, is that it occurs in such a diverse range of systems - with completely different sizes, structures and microscopic parameters [6–8, 25]. This diversity, in turn, leads to a rich variety of observable, complex behaviour. Hence, instead of identifying specific quantum systems and regions of parameter space where a synchronised response can be observed, we consider it pertinent to take a different route and determine, more generally, conditions which will ensure synchronisation in a quantum system.

In this work we adopt this approach, identifying these conditions and uncovering a novel mechanism which guarantees synchronisation in a generic open quantum system. This mechanism is based solely on symmetry and is thus independent of the system’s microscopic details. More specifically, these conditions describe the existence of a strong dynamical symmetry operator [26] which, when present, underpins the formation of a structure to the long-time density matrix which ensures limit cycles describing entangled, cooperative behaviour. These cycles capture the essence of quantum synchronisation, describing oscillations where the constituents of the system are locked to a common phase and frequency whilst also featuring the off-diagonal long-range order present in states such as BECs and superconductors [27, 28]. Furthermore, we prove this behaviour is, to first order, completely robust to the presence of symmetry-breaking perturbations.

We then use this understanding of synchronisation in terms of dynamical symmetries to identify several physical systems, which have no classical analogue, where this phenomenon arises - a chain of interacting spin 1s and the many-body charge-dephased Hubbard model. These systems exhibit perfect distance-invariant phase synchronisation for a wide range of parameters and ini-

tial states. Moreover, their strong dynamical symmetries allow us to identify analytical expressions for the long-time density matrix - which is typically an unfeasible task in strongly-correlated many-body systems. Finally, we perturb these systems away from the dynamical symmetry regime where the non-linear response facilitates the observation of strong, exceptionally long-lived signatures of both phase and frequency locking.

## II. SYNCHRONISATION IN GENERIC QUANTUM SYSTEMS

### A. Strong Dynamical Symmetries

Firstly, we introduce the concept of a strong dynamical symmetry by providing a brief summary of the work in [26]. This concept applies in both Markovian and non-Markovian regimes, here we restrict ourselves to Markovian dynamics for simplicity. Consider the time evolution of the density matrix of an open quantum system via the Lindblad equation (here, and in the remainder of this work, we set  $\hbar = 1$ )

$$\begin{aligned} \frac{\partial \rho}{\partial t} &= \mathcal{L}\rho = -i[H, \rho] + \sum_j \gamma_j (L_j \rho L_j^\dagger - \frac{1}{2} \{L_j^\dagger L_j, \rho\}), \\ &= -i[H, \rho] + D[\rho], \end{aligned} \quad (1)$$

where  $H$  is the Hamiltonian of the system and  $\{L_j\}$  are a set of ‘jump’ operators which model the interaction between the system and the environment with associated coupling strengths  $\{\gamma_j\}$ . The jump operators are used to form the dissipator  $D[\rho]$  which competes with the coherent evolution due to the Hamiltonian  $H$ . We denote the Liouvillian superoperator with  $\mathcal{L}$  and the steady state(s) as  $\rho_{ss}$ , which satisfy  $\mathcal{L}\rho_{ss} = 0$ .

If we can identify an operator  $A$  which satisfies

$$[H, A] = \omega A, \quad [L_j, A] = [L_j^\dagger, A] = 0 \quad \forall j, \omega \in \mathbb{R} \quad (2)$$

then we say that the system possesses a ‘strong dynamical symmetry’. The relation  $[H, A] = \omega A$  describes the presence of a dynamical symmetry operator. We then refer to this as a strong dynamical symmetry operator because it commutes with all the jump operators and their conjugates [29].

It is then straightforward to prove from these relations that there exists a series of eigenmodes of  $\mathcal{L}$  of the form

$$\rho_{n,m} \propto (A)^n \rho_{ss} (A^\dagger)^m, \quad \mathcal{L}\rho_{n,m} = i\omega(m-n)\rho_{n,m}, \quad (3)$$

where the corresponding imaginary eigenvalues indicate the presence of non-stationary dynamics in the long-time limit of the system. The operator  $A$  acts as a raising/lowering operator, generating a ladder of equidistant mixed states within the kernel of the Liouvillian. These results extend beyond that of a decoherence free subspace [30, 31] as the imaginary modes are, in general,

mixed and cannot be written as a convex superposition of pure states  $|\phi\rangle\langle\phi|$  which are immune to the dissipation  $L_j|\phi\rangle = 0 \quad \forall j$ .

### B. Quantum Synchronisation via Dynamical Symmetries

We now show how systems which possess a strong dynamical symmetry provide a natural environment for observing quantum synchronisation. Consider an interacting, open quantum system where the Hilbert space is constructed from a series of  $N$  local spaces or ‘bodies’  $\mathcal{H} = \otimes_j \mathcal{H}_j$ . We assume that the environment interacts with the system in a local, translationally-invariant manner, i.e. the  $L_j$  in Eq. (1) are purely local and each site experiences the same jump operators and dissipation rates.

We now imagine the system has a strong dynamical symmetry operator satisfying Eq. (2) and assume the imaginary modes from Eq. (3) form a complete basis for the long-time density matrix of the system. Consequently, we can write this state as

$$\lim_{t \rightarrow \infty} \rho(t) = \sum_{\substack{n,m \\ n \geq m}} \left( C_{n,m} e^{i\omega(m-n)t} \rho_{n,m} + \text{h.c.} \right), \quad (4)$$

where the  $C_{n,m}$  are a set of real coefficients associated with the overlap between the initial state and the  $\rho_{n,m}$ . Now, consider the expectation value of some  $N$ -point observable  $X = \prod_{j \in B} X_j$ , where  $B = \{a, b, c, \dots\}$  is a set of  $M$  local spaces containing no duplicates and  $X_j$  is some hermitian local operator acting on site  $j$ . It follows from Eq. (4) that

$$\lim_{t \rightarrow \infty} \langle X \rangle(t) = \sum_{\substack{n,m \\ n > m}} D_{n,m} \cos(\omega(m-n)t) + \text{const.}, \quad (5)$$

with  $D_{n,m} = 2\text{Tr}(X\rho_{n,m})C_{n,m}$ . Provided that  $D_{n,m} \neq 0$  for at least one  $n, m$  where  $|n-m| = 0$  then Eq. (5) describes coherent, non-decaying limit cycles in the associated observable. The equidistance of the imaginary eigenspectrum is crucial and ensures the frequencies involved are commensurate and do not destructively interfere with each other. These limit cycles, along with the well-defined, coherent phase-evolution described in Eq. (4) are hallmark features of temporal synchronisation.

Importantly, because the environmental interaction with the system is local and translationally-invariant the dephasing can often ‘wash’ out any geometry associated with the system, creating entangled steady states which have no identifiable length-scale and completely uniform off-diagonal long-range order [26, 32]. Through Eq. (3) the  $\rho_{n,m}$  inherit these features and the resulting limit cycles in Eq. (5) describe perfect, distance-invariant, entangled synchronisation between the involved bodies - regardless of the specific initial state or parameters of the model; the only requirement is that one of the coefficients  $D_{n,m} \neq 0$ . As we will illuminate with a pair

of examples in Sec. III these distance-invariant cycles cannot be fully captured with a mean-field approach and describe intrinsically quantum behaviour.

### C. Perturbations away from the Dynamical Symmetry Regime

We now show how this synchronisation is robust to perturbations away from the dynamical symmetry regime. Typically, we can imagine that the relation  $[H, A] = \omega A$  from Eq. (2) arises due to some homogeneous field  $F = \omega \sum_j f_j$  in the Hamiltonian for which  $A$  is a raising/lowering operator. The synchronisation described in the previous section is then a consequence of perfect phase locking of the individual constituents of the systems, frequency locking will occur because the individual modes  $j$  share the same natural frequency  $\omega$ .

If the field is not homogeneous, i.e.  $F = \sum_j \omega_j f_j$ , then the Hamiltonian  $H$  can be split into two terms. The first contains a homogeneous term  $\sum_j \bar{\omega}_j f_j$  and all other non-field terms, the second contains only the inhomogeneous part  $\sum_j \delta_j f_j$ . We have parametrised  $\omega_j$  as  $\omega_j = \bar{\omega}_j + \delta_j$  where  $\bar{\omega}_j$  is the average of the set  $\{\omega_j\}$ . We then, correspondingly, split the Liouvillian into two parts and scale by  $1/\bar{\omega}_j$ :

$$\begin{aligned} \mathcal{L} &= \mathcal{L}^{(0)} + \epsilon \mathcal{L}^{(1)}, \\ \mathcal{L}^{(0)} &= -\frac{i}{\bar{\omega}_j} [H - \sum_j \delta_j f_j, \cdot] + \frac{1}{\bar{\omega}_j} D[\cdot], \\ \mathcal{L}^{(1)} &= -i \left[ \sum_j \frac{\delta_j}{\bar{\omega}_j} f_j, \cdot \right], \end{aligned} \quad (6)$$

where  $\epsilon = \bar{\delta}_j/\bar{\omega}_j$  is the, small, perturbation parameter and  $\bar{\delta}_j$  is the average over the set of detunings  $\{\delta_j\}$ . We then assume that the eigenvectors and eigenvalues of this new Liouvillian are perturbations on those for  $\mathcal{L}^{(0)}$ :

$$\begin{aligned} \rho &= \rho^{(0)} + \epsilon \rho^{(1)} + \epsilon^2 \rho^{(2)} + \dots, \\ \lambda &= \lambda^{(0)} + \epsilon \lambda^{(1)} + \epsilon^2 \lambda^{(2)} + \dots \end{aligned} \quad (7)$$

It then follows (see Supplemental Material, SM) that the first order eigenvalue shift is  $\lambda^{(1)} = \text{Tr} \left[ (\rho^{(0)})^\dagger \mathcal{L}^{(1)} \rho^{(0)} \right]$ , which is purely imaginary as it can be rearranged to be the trace of a skew-hermitian matrix. As a result, to first order, the eigenvalues of the eigenmodes in Eq. (3) remain imaginary and thus there is no decay in the system's long-time dynamics when perturbed away from the dynamical symmetry regime.

Moreover, if the imaginary eigenmodes are unchanged under a swap between two bodies  $j$  and  $l$  then we have that  $\lambda^{(1)} = 0$  as  $\text{Tr} \left[ (\rho^{(0)})^\dagger f_j \rho^{(0)} \right]$  is independent of  $j$ . As discussed in Sec. II B this symmetry in the imaginary modes is often seen for local, translationally-invariant dephasing [26, 32]. Hence, the system will undergo completely non-linear response to perturbations away from

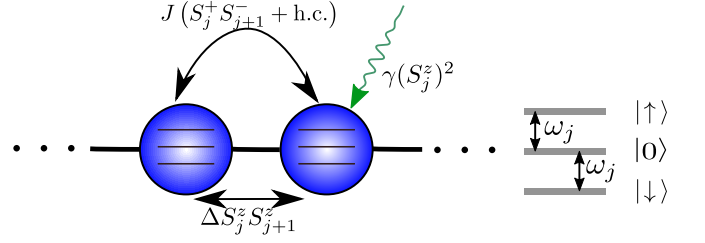


FIG. 1. Series of spin-1s in a chain geometry. The system is governed by the Hamiltonian in Eq. (37) with on-site dephasing of the form  $L_j = (S_j^z)^2$ . The resulting dynamics is described by the Master Equation in Eq. (27).

the dynamical symmetry regime. To first order, the solutions in Eq. (3) are still eigenmodes and we can expect to observe the corresponding synchronised features these eigenmodes possess, with a lifetime that scales at least quadratically with the perturbation parameter  $\epsilon$ . The individual constituents will be locked in both phase and frequency, despite having different natural frequencies.

## III. EXAMPLES

We have shown how, in a generic interacting open quantum system, the presence of a strong dynamical symmetry underpins a coherent, typically distance-invariant, synchronised structure to the long-time density matrix. Furthermore, the system is robust to perturbations away from the dynamical symmetry regime. In order to elucidate these results we present a pair of paradigmatic examples where they can be observed.

### A. Synchronisation in a chain of Spin-1s

For our first example, we take a system formed from a series of spin-1s or qutrits. The local basis for each spin-1 is spanned by the three states  $\{|\downarrow\rangle, |0\rangle, |\uparrow\rangle\}$ . The key operators are  $S_j^+$ ,  $S_j^-$  and  $S_j^z$  which are, respectively, the spin-1 raising, lowering and magnetisation operators for spin  $j$ . The  $x$  and  $y$  components of the spin-1 operator can be formed from the raising and lowering operators:  $S_j^x = (1/2)(S_j^+ + S_j^-)$ ,  $S_j^y = (i/2)(S_j^- - S_j^+)$ . By dropping the site subscript we denote the total of an operator, e.g.  $S^z = \sum_j S_j^z$ .

We take a spin-1 anisotropic Heisenberg model in a chain geometry [33] (see Fig. 1)

$$H = \sum_{j=1}^N \omega_j S_j^z + \sum_{j=1}^{N-1} J(S_j^+ S_{j+1}^- + S_j^- S_{j+1}^+) + \Delta S_j^z S_{j+1}^z, \quad (8)$$

where the spins each have natural frequency  $\omega_j$  and nearest-neighbour coupling strengths  $J$  and  $\Delta \neq 0$ . The system is then immersed in a bath which induces local,

quadratic dephasing in a spin-agnostic manner. The ensuing dynamics is modelled via the equation

$$\frac{\partial \rho}{\partial t} = \mathcal{L}\rho = -i[H, \rho] + \gamma \sum_{j=1}^N (S_j^z)^2 \rho (S_j^z)^2 - \frac{1}{2} \{ (S_j^z)^4, \rho \}, \quad (9)$$

which is the Master equation in Eq. (1) with jump operators  $L_j = (S_j^z)^2$  applied to each spin at a rate  $\gamma \forall j$ .

Initially, in order to derive an analytical solution to the long-time dynamics, we focus on the ‘frequency-matched’ case  $\omega_j = \omega, \forall j$ . In the SM we prove that the steady state can always be written in the form

$$\rho_{ss} = \sum_{m=-N}^N \lambda_m \left( \sum_i |m_i\rangle \langle m_i| \right) + \lambda'_0 \sum_i |0_i\rangle \langle 0'_i|, \quad (10)$$

where  $|m_i\rangle$  is an eigenvector of  $S^z$  with eigenvalue  $m$ :  $S^z |m_i\rangle = m |m_i\rangle$ , and  $i$  indexes the possible eigenvectors for each  $m$ . We have also defined  $|-m'_i\rangle = \text{SF} |m_i\rangle$ , where  $\text{SF} = \otimes_{j=1}^N (|\uparrow\rangle \langle \downarrow| + |\downarrow\rangle \langle \uparrow| + |0\rangle \langle 0|)$  is the spin-flip operator. For example if  $|2_1\rangle = |0 \uparrow \uparrow\rangle$  then  $|-2'_1\rangle = |0 \downarrow \downarrow\rangle$ , or if  $|0_2\rangle = |0 \uparrow \downarrow\rangle$  then  $|0'_2\rangle = |0 \downarrow \uparrow\rangle$ . In order for  $\text{Tr}(\rho_{ss}) = 1$  the elements  $\{\lambda_m\}$  and  $\lambda'_0$  must satisfy the equation

$$\lambda'_0 + \sum_{m=-N}^N \lambda_m \sum_{s=0}^N \binom{N}{s} \binom{N-s}{(N-s+m)/2} = 1, \quad (11)$$

where the terms in the second summation are skipped if  $(N-s+m)/2$  is not an integer.

The long-time dynamics of  $\mathcal{L}$  is not, however, solely governed by this steady state. We identify (see SM) multiple strong dynamical symmetry operators of the form

$$A_m = \sum_i |m_i\rangle \langle -m'_i|, \quad m \neq 0, m = -N, \dots, N, \quad (12)$$

which each satisfy Eq. (2)

$$[H, A_m] = 2m\omega A_m, \quad [L_j, A_m] = [L_j^\dagger, A_m] = 0, \quad \forall j. \quad (13)$$

Following this we can determine, see Eq. (3), the imaginary eigenmodes of the Liouvillian through the action of these operators on the steady state. Explicitly, we have,

$$\rho_{1,0}^m \propto A_m \rho_{ss} \propto A_m, \quad \mathcal{L} \rho_{1,0}^m = -2im\omega, \quad (14)$$

which is a non-trivial result as the steady-state  $\rho_{ss}$  is inherently singular. Further application of  $A_m$  is redundant as  $A_m A_m = 0$  and thus, each  $A_m$  generates a unique imaginary eigenmode  $\rho_{1,0}^m$  via left-multiplication of the steady-state. Crucially, however, the eigenspectrum is still equidistant as the eigenvalues of the different modes form a ladder with a spacing of  $2\omega$ . Hence, the structure of the long-time eigenspace is analogous to a system with a single strong dynamical symmetry operator.

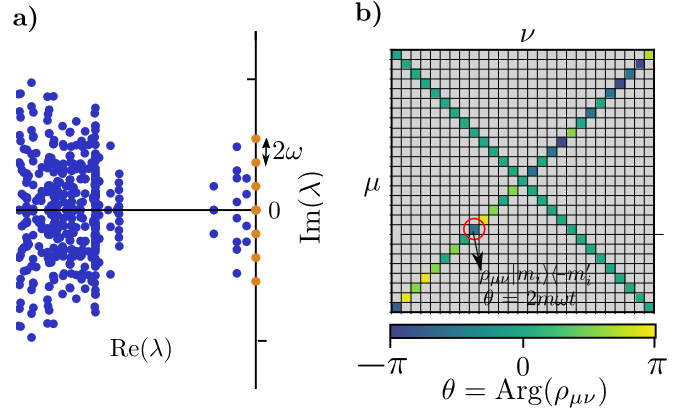


FIG. 2. (a) Eigenvalues  $\{\lambda\}$  close to the real axis for the Liouvillian superoperator from the Master Equation in Eq. (27). Parameters are  $N = 3$ ,  $\omega_j = 1.0J \forall j$ ,  $\Delta = 0.5J$ ,  $\gamma = 2.0J$ . Eigenvalues with  $\text{Re}(\lambda) = 0$  are marked in orange, all others are marked in blue. (b) Structure of the density matrix at time  $tJ = 100.0$  under the map in Eq. (27) with the same parameters as in a). Initial state is a random product state. The colour indicates the phase of each complex element  $\rho_{\mu\nu}$ , the grey colour indicates  $\text{Abs}(\rho_{\mu\nu}) = 0$  and so the phase is not plotted. The indices  $\mu$  and  $\nu$  run over the basis vectors of the Hilbert space in lexicographic order when they are converted to ternary strings with  $\uparrow = 2, 0 = 1, \downarrow = 0$ . As an example when  $\mu = 1$  this corresponds to the basis vector  $|\uparrow\uparrow\uparrow\rangle = |222\rangle$  and when  $\mu = 27$ :  $|\downarrow\downarrow\downarrow\rangle = |000\rangle$ . Example element (ringed in red) has a phase which evolves in time as  $\theta = 2m\omega t$  where  $m$  is the magnetisation of the corresponding basis vector  $|m_i\rangle \langle -m'_i|$ .

The steady state and imaginary eigenmodes in Eqs. (30) and (12) form a complete basis for the long-time dynamics of Eq. (27) and so, similarly to Eq. (4), the density matrix can be expressed as a superposition of these modes in the limit  $t \rightarrow \infty$ . The imaginary modes describe coherences between sectors of opposite magnetisation, their excitation will ensure the system reaches a limit cycle in the long-time limit. Moreover, the density matrix is completely translationally invariant, the off-diagonal coherences described in Eq. (3) occur at all length-scales of the chain and are completely uniform with respect to distance.

In Fig. 2 we visualise the analytical results in Eqs. (30), (12) and (14). We present a plot of the eigenspectrum of  $\mathcal{L}$  [Fig. 2(a)], the formation of these imaginary eigenmodes is clear and their spacing is set by the value of  $\omega$ . We also show the structure of the density matrix in the long-time limit of Eq. (27) [Fig. 2(b)]. The system is in a superposition of the steady state in Eq. (30) and the imaginary modes in Eq. (12), hence it only has elements along the diagonal and anti-diagonal in the configuration basis. The magnitude of each of these matrix elements is constant in time. The phase of the elements along the anti-diagonal is well-defined and evolves in time at a frequency  $f = 2m\omega$  for the corresponding matrix element  $|m_i\rangle \langle -m'_i|$ .

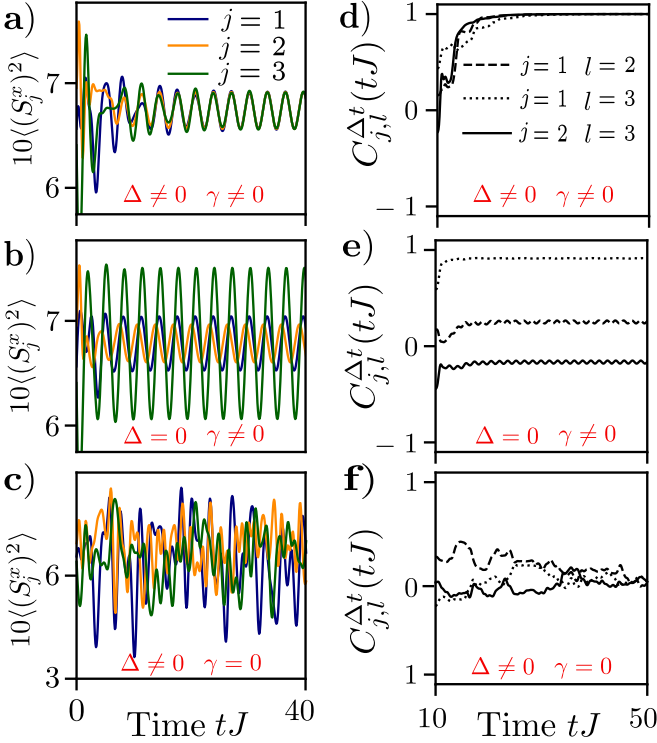


FIG. 3. (a-c) Dynamics of  $\langle (S_j^x)^2 \rangle$  for a quench from a completely random product state under the map in Eq. (27) with  $N = 3$ ,  $\omega_j = 1.0J \forall j$ . a)  $\Delta = 0.5J$ ,  $\gamma = 1.0J$ , b)  $\Delta = 0$ ,  $\gamma = 2.0J$  c)  $\Delta = 0.5J$ ,  $\gamma = 0$ . (d - f) Pearson time-correlation coefficient for each possible pair of functions from the respective plots in (a-c). The time-averaged window is a rolling window with width  $\Delta t = 10.0tJ$  centred at time  $tJ$ .

We can explicitly prove that this coherent density matrix structure leads to observable synchronisation in the long-time limit of the system. Specifically, consider the operator  $X = \prod_{j \in B} (S_j^x)^2$ , where  $B = \{a, b, c, \dots\}$  is a set of  $M$  sites containing no duplicates. The operator is formed from quadratic, local operators which measure fluctuations in the magnetisation. The quadratic form is necessary in order to be able to measure the coherences between the basis states  $|\downarrow\rangle$  and  $|\uparrow\rangle$  - any operator formed solely from linear local operators will relax to stationarity. We prove (see SM) that in the limit  $t \rightarrow \infty$

$$\langle X \rangle = D_0 \text{Tr}(\rho_{ss} X) + \sum_{m=1}^M D_m \cos(2m\omega t) \text{Tr}(\rho_{1,0}^m X), \quad (15)$$

where the real coefficients  $D_m$  are those associated with the overlap between the initial state  $\rho(0)$  and either the imaginary eigenmodes or the steady state. The trace overlap  $\text{Tr}(\rho_{1,0}^m X)$  only depends on the cardinality of  $B$ , not the specific sites within the set; a direct consequence of the complete translational invariance of the modes spanning the kernel. Consequently  $\langle X \rangle$  is also independent of the specific choice of sites over which we measure the correlator  $X$ , only the number of sites matters.

Thus we see that the long-time dynamics will perfectly synchronise the spin-1s to clean, coherent limit-cycles - regardless of the specifics of the initial state or the Hamiltonian parameters.

Moreover, the modes in Eq. (12) are entangled and cannot be written as a superposition of separable states - which we explicitly show in the following numerics. We also demonstrate that the reduced correlator  $\langle X \rangle - \prod_{j \in B} \langle X_j \rangle$  is distance-invariant and non-zero. Hence, we consider the synchronisation observed in Eq. (15) to be inherently quantum with the underlying long-range correlations not obtainable via a mean field approach.

All of these results are valid for any arbitrary length chain of  $N$  spin-1s under the Liouvillian in Eq. (27). In the subsequent numerics we focus on a small series of spin-1s, i.e.  $N = 3$  or  $N = 4$ . This is because as the system sizes increases, for generic initial states (product states for example), the diagonal correlations become increasingly dominant in the long-time limit compared to the off-diagonal coherences ( $|D_0| \gg |D_{m \neq 0}|$ ). Hence, we can readily resolve features of quantum synchronisation by focussing on a small chain. Furthermore this allows us to directly witness our analytical calculations by solving the Master equation in Eq. (27) through numerical exponentiation of the Liouvillian superoperator  $\mathcal{L}$ .

For the following results, we start in a specified initial state and then time-evolve it under the Liouvillian in Eq. (27) measuring various time-dependent quantities in order to observe the formation of synchronisation. As a first synchronisation measure for the local observables in our model we consider the time-dependent Pearson-correlation factor [14, 34]. It can be used to measure the correlation over time for two functions  $f, g$  defined on a domain  $[t, t + \Delta t]$

$$C_{f,g}^{\Delta t}(t) = \frac{\int_t^{t+\Delta t} (f - \bar{f})(g - \bar{g}) dt}{\sqrt{\int_t^{t+\Delta t} (f - \bar{f})^2 dt \int_t^{t+\Delta t} (g - \bar{g})^2 dt}}, \quad (16)$$

with the function average  $\bar{f} = \frac{1}{\Delta t} \int_t^{t+\Delta t} f dt$ . This correlation factor is maximal (minimal), 1 (-1) when the two signals  $f$  and  $g$  are perfectly synchronised (anti-synchronised), and 0 when they display no correlations.

In Fig. 3 we set  $f = \langle (S_j^x)^2 \rangle$  and  $g = \langle (S_l^x)^2 \rangle$  in order to measure the synchronisation over time between two of the spin-1s  $j$  and  $l$  - we start from a completely random product state. We also include the individual functions  $\langle (S_j^x)^2 \rangle$  over time for each spin. In agreement with Eq. (15), when both the environment and interactions are present ( $\gamma, \Delta \neq 0$ ) the dynamics causes the spins to synchronise perfectly [Figs. 3(a) and (d)] to the same frequency and phase, despite being initialised with random phases. The frequency of the oscillations is directly determined by the equidistant spacing of the imaginary eigenvalues. For comparison [Fig. 3(b)] we show the case when the environment is present but there are no interactions ( $\gamma \neq 0, \Delta = 0$ ). The presence of dissipation causes the system to converge to the expected clean coherent limit cycles [26] but the limit cycles for each spin are out



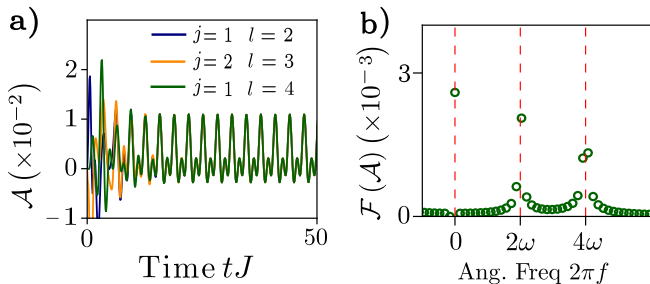


FIG. 4. Dynamics of  $\mathcal{A} = \langle (S_j^x)^2 (S_l^x)^2 \rangle - \langle (S_j^x)^2 \rangle \langle (S_l^x)^2 \rangle$  for a quench from a random state with total  $x$ -magnetisation  $\langle S^x \rangle = 0$  under the map in Eq. (27) with  $N = 4$ ,  $\omega_j = 1.0J \forall j$ ,  $\Delta = 0.5J$ ,  $\gamma = 2.0J$  b) Amplitude of the Fourier transform  $\mathcal{F}(\mathcal{A})$  versus angular frequency in the long-time limit. The red-dashed lines indicate the expected angular frequency response based on Eq. (15). Only a selection of the possible values of  $j$  and  $l$  are shown for brevity.

of phase. The absence of interactions prevents perfect synchronisation as the kernel of the Liouvillian still has a memory of the initial geometry of the system. We also show the closed case when  $\gamma = 0$  [Figs. 3(c) and (f)], the dynamics are completely chaotic and unsynchronised due to the multitude of incommensurate frequencies in the eigenvalues of the Hamiltonian.

Whilst the plots in Fig. 3 demonstrate that the spins are able to perfectly lock phases they do not capture the collective origin of this synchronisation. In this vein, in Fig. 4, we plot the reduced correlator  $\mathcal{A} = \langle (S_j^x)^2 (S_l^x)^2 \rangle - \langle (S_j^x)^2 \rangle \langle (S_l^x)^2 \rangle$ , which is non-zero and identical for any choice of spins  $j$  and  $l$ . The observed oscillations contain several frequencies [Fig. 4(b)] due to the excitement of multiple imaginary modes in Eq. (12). These imaginary modes all contain coherences between different spins, the synchronisation observed in Fig. 3 is dependent on the existence of these inter-spin coherences and Fig. 4 shows that they give rise to perfect, distance-invariant correlations throughout the system.

So far we have considered the ‘homogeneous’ case  $\omega_j = \omega \forall j$ . The spins share the same natural frequency and we have shown how, under dephasing and interactions, their phases will align perfectly. In order to discuss synchronisation in full we now set the frequencies of the spins to be mismatched. In this case, the imaginary modes in Eq. (3) are no longer exact eigenvectors of the Liouvillian and, in the long-time limit, the system will decay to an ensemble which is diagonal in the configuration basis - where no synchronisation can occur. However, as was shown in Eq. (6), for sufficiently small values of  $\epsilon$ , the system is only slightly perturbed from a ‘dynamical symmetry’ regime defined by the spins having a common frequency which is the average of their natural frequencies. Furthermore, through Sec. II C we know the system is, to first order, robust to this kind of perturbation. Hence, it is interesting to observe whether the spins are able to synchronise to the dynamical symmetry regime on an intermediate time-scale and, if so, how long

the system takes to desynchronise and reach a diagonal ensemble.

As measures to track this, and to highlight the quantum nature of the synchronisation in Figs. 3 and 4, we introduce two common witnesses for quantum synchronisation: the negativity  $\mathcal{N}$  [35] and off-diagonal coherences  $\mathcal{C}$  [11]

$$\mathcal{N}_j(\rho) = \frac{\|\rho^{T_j}\| - 1}{2},$$

$$\mathcal{C} = \sum_{i \neq j} |\rho_{ij}|, \quad (17)$$

with  $T_j$  indicating the partial transpose with respect to site  $j$  and  $\|X\| = \text{Tr} \sqrt{X^\dagger X}$  denoting the trace norm of an operator. The negativity can be seen as a measure of the degree to which spin  $j$  is entangled with the rest of the system whilst the coherence quantifier  $\mathcal{C}$  describes the total magnitude of the off-diagonal elements in the density matrix. When the frequencies are matched the system is synchronised, and due to the off-diagonal, entangled nature of the modes in Eq. (3) quantities such as these will remain finite indefinitely.

In Fig. 5 we show how these synchronisation witnesses evolve in time when the system is perturbed from the dynamical symmetry regime. We use the detuning strength  $\delta$  to characterise the range of the natural frequencies. The explicit distribution of natural frequencies is not important, the key parameter is its width and in the SM we obtain similar results when the natural frequencies are drawn from a uniform random distribution. Initially, the system is in a product state where  $\mathcal{N} = 0$ , the transient dynamics then causes the formation of entanglement and anti-diagonal coherences which decay away at a rate set by  $\delta$ . We show how this entanglement forms [Figs. 5(c-d)]: despite having mismatched frequencies and phases the spins lock to an intermediate limit cycle with identical phase and frequency - which is twice the average of the natural frequencies  $\bar{\omega}_j$  (due to the factor of 2 in Eq. (13)). The life-time of this cycle is large and as  $\delta \rightarrow 0$  diverges to infinity, evidenced by the tongue-like behaviour seen in Figs. 5(a-b). These figures show how the corresponding measures act as strong witnesses to the synchronisation in the system - emphasizing its quantum nature.

The imaginary eigenmodes in Eq. (3) are translationally-invariant and hence the robust, synchronised behaviour observed [Fig. 5] is the result of a second-order response to the detuning. The cross-sections included in Fig. 5b are evidence of this. At a given time the coherences are well-approximated by a gaussian profile (see SM) as a function of the detuning. Meanwhile at a given detuning the coherences decay away exponentially as a function of time, the decay rate  $d$  is proportional to the square of the detuning (see SM for numerical evidence of this). Furthermore, we explicitly show this non-linear scaling in Fig. 6. We calculate the shift in the imaginary eigenvalues,  $|\lambda - \lambda^{(0)}|$  (see Sec. II C) from

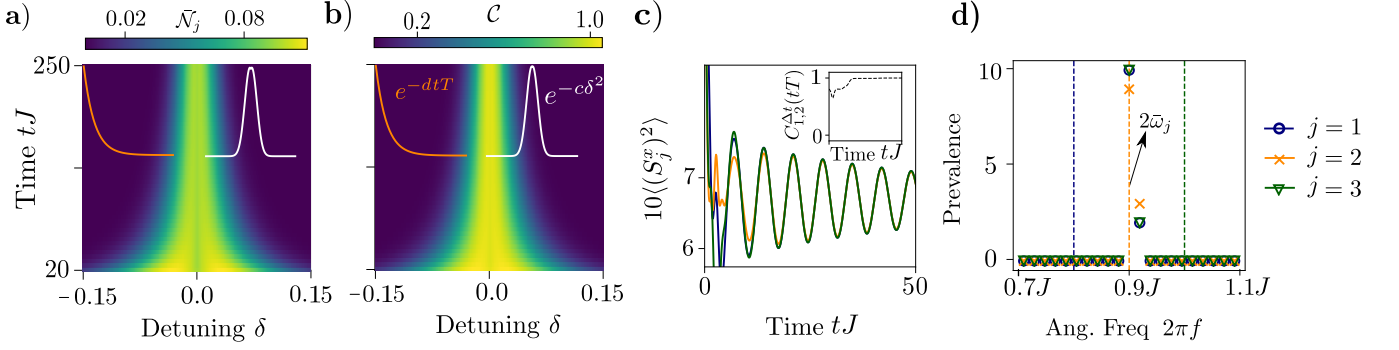


FIG. 5. a-b) Plot of synchronisation witnesses vs time and detuning for the Master Equation in Eq. (27) with  $N = 3$ . The system is initialised in the state  $|\psi(0)\rangle = |\rightarrow 00\rangle$ , where  $|\rightarrow\rangle = \frac{1}{\sqrt{2}}(|\uparrow\rangle + |\downarrow\rangle)$ , and evolved in time with parameters  $\{\omega_1, \omega_2, \omega_3\} = \{1.0 - \delta, 1.0, 1.0 + \delta\}J$ ,  $\gamma = 2.0J$ ,  $\Delta = 0.5J$ . Insets, top-left) Cross-section (orange) of these measures versus time at detuning  $\delta = -0.075$ . top-right) Cross-section (white) of these measures versus detuning at time  $tJ = 250.0$ . The parameters  $d$  and  $c$  are constants used to parametrise the cross-sections (see SM). a) Synchronisation is measured by the average negativity, see Eq. (17), for each site. b) Synchronisation is measured as the total magnitude of the off-diagonal coherences, see Eq. (17). (c) Example dynamics of  $\langle(S_j^x)^2\rangle$  for the same system except with specific natural frequencies  $\{\omega_1, \omega_2, \omega_3\} = \{0.4, 0.45, 0.5\}J$  and dephasing  $\gamma = 1.0J$ . Inset) Pearson Coefficient, see Eq. (16), for the two functions  $\langle(S_1^x)^2\rangle$  and  $\langle(S_2^x)^2\rangle$  from time  $tJ = 5$  to  $tJ = 20$ . d) Prevalence of angular frequencies, extracted from the distribution of angular frequencies created using the time-periods between successive turning points for the oscillations in c) but up to  $tJ = 100.0$ . Dashed lines indicate the expected delta function in the prevalence, based on each spin's natural frequency. The central line is twice the average of the natural frequencies  $\bar{\omega}_j$ .

their original value  $\lambda^{(0)}$  at  $\delta = 0$  as a function of the detuning  $\delta$ . There is no noticeable shift to first order in  $\delta$  - the fitted curve is proportional to  $\delta^2$ . Notably, the highest imaginary eigenmode  $\rho_{1,0}^N = |\uparrow\uparrow\dots\rangle\langle\downarrow\downarrow\dots|$  is always unshifted, and remains imaginary regardless of the

distribution of natural frequencies.

## B. Many-body synchronisation in the Hubbard model

As our second example, we take the 1D  $N$ -site Hubbard model [36] in, potentially, disordered magnetic and chemical fields. We focus on 1D lattices for numerical tractability, nonetheless it should be emphasized that these results are solely based on symmetry and thus can be observed in any bi-partite  $d$ -dimensional realisation of the Hubbard model. The Hamiltonian reads

$$H = -\tau \sum_{\langle j,l \rangle, \sigma} (c_{\sigma,j}^\dagger c_{\sigma,l} + \text{h.c.}) + U \sum_j n_{\uparrow,j} n_{\downarrow,j} + \sum_j \omega_j (n_{\uparrow,j} - n_{\downarrow,j}) + \sum_j \mu_j (n_{j,\uparrow} + n_{j,\downarrow}), \quad (18)$$

where  $c_{\sigma,j}^\dagger$  and its adjoint are the usual creation and annihilation operators for a fermion of spin  $\sigma \in \{\uparrow, \downarrow\}$  on site  $j$ . Additionally,  $n_{\sigma,j}$  is the number operator for a particle of spin  $\sigma$  on site  $j$  and  $\tau$ ,  $U$ ,  $\omega_j$  and  $\mu_j$  play the role of kinetic, interaction, magnetic and chemical energy scales respectively.

We then couple the system to a bath which induces spin-agnostic dephasing on each site. Hence, the system's time evolution can be described by the Lindblad

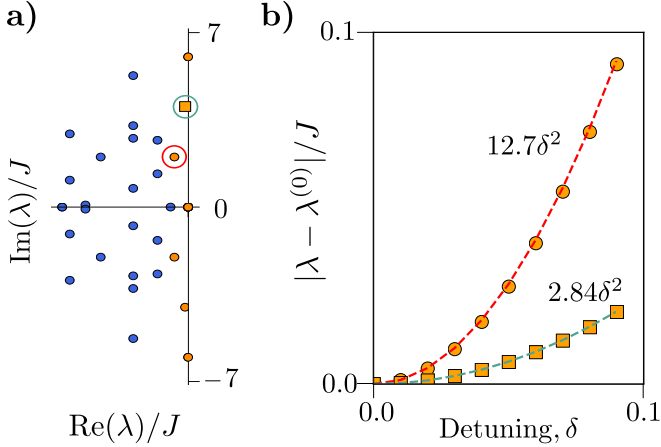


FIG. 6. a) Spectrum of eigenvalues close to the real axis for the Liouvillian in Eq. (27) with  $\Delta = 0.5J$ ,  $\gamma = 2.0J$ ,  $\{\omega_1, \omega_2, \omega_3\} = \{1.0 - \delta, 1.0, 1.0 + \delta\}J$  and  $\delta = 0.07$ . Orange coloured eigenvalues are those which lie on the imaginary axis when  $\delta = 0$ , they are shifted from the axis due to the finite value of  $\delta$ . (b) Scaling of the distance shifted  $|\lambda - \lambda^{(0)}|$ , in the complex plane, as a function of  $\delta$ , where  $\lambda$  is the new eigenvalue and  $\lambda^{(0)}$  is the original imaginary eigenvalue when  $\delta = 0$ . Curves are for the two circled eigenvalues in a), which shows the specific example  $\delta = 0.07$ . Dashed curves are quadratic fits.

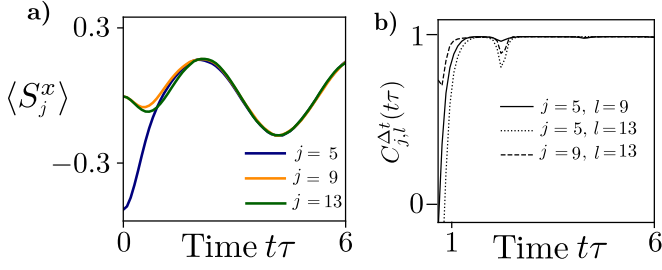


FIG. 7. a) Dynamics of  $\langle S_j^x \rangle$  for a quench of the  $N = 15$  site charge-dephased Hubbard model described by the Master Equation in Eq. (19). Parameters are  $\gamma = 2.5\tau$ ,  $U = 1.0\tau$ ,  $\omega_j = 1.5\tau \forall j$ ,  $\mu_j \in \text{Rand}[0.0, 0.2]\tau$  where  $\text{Rand}[0.0, 0.2]\tau$  is a uniformly-drawn random number on the specified interval. The initial state is  $|\psi(0)\rangle = \bigotimes_{j=1}^5 |\chi\rangle$  where  $|\chi\rangle = |\leftarrow\downarrow\uparrow\rangle$  and  $\rightarrow, \leftarrow, \uparrow$  and  $\downarrow$  correspond to each site being polarised in the positive  $x$ -direction, negative  $x$ -direction, positive  $z$  and negative  $z$ -direction respectively. b) Pearson time-correlation coefficient for each possible pair of functions from a). The time-averaged window is a rolling window with width  $\Delta t = 0.5t\tau$  centred at time  $t\tau$ .

Equation:

$$\frac{\partial \rho}{\partial t} = \mathcal{L}\rho = -i[H, \rho] + \gamma \sum_{j=1}^N n_j \rho n_j - \frac{1}{2} \{(n_j)^2, \rho\},$$

$$n_j = n_{j,\uparrow} + n_{j,\downarrow}. \quad (19)$$

The case  $\omega_j = \omega \forall j$  of this model was originally studied in Ref. [26]. In this regime the system is known to possess a strong dynamical symmetry as the magnetic field breaks the spin  $\text{SU}(2)$  symmetry of the model:  $[H, S^\pm] = \omega S^\pm$ ,  $[L_j, S^\pm] = 0 \forall j$ , where  $S^+ = \sum_j c_{j,\uparrow}^\dagger c_{j,\downarrow}$  is the global magnetic raising operator. In this case there is a single strong dynamical symmetry operator which can be used to form the set of equidistant imaginary eigenmodes

$$\rho_{nm} \propto (S^+)^n \rho_{ss} (S^-)^m, \quad \mathcal{L}\rho_{nm} = i\omega(m - n)\rho_{nm}. \quad (20)$$

These modes cause the existence of a persistent limit cycles in the magnetisation (in the  $x$  and  $y$  directions) of the system. For example, by defining the operator  $X = \prod_{j \in B} S_j^x$  (where  $B = \{a, b, c, \dots\}$  is a set of  $M$  sites containing no duplicates) we can use Eq. (5) to prove (see SM):

$$\lim_{t \rightarrow \infty} \langle X \rangle(t) = \sum_{i=0}^{\lfloor M/2 \rfloor} D_i \cos((2i + d)\omega t), \quad d = M \bmod 2, \quad (21)$$

where the coefficients  $D_i$  are set by the initial state of the system. The imaginary modes in Eq. (20) are completely translationally symmetric (see Ref. [26] for the explicit form of the steady state) and thus this observable is dependent only on the cardinality  $M$  of the set  $B$ , not the specific sites within the set.

As a result, even in the presence of disorder in the chemical potential, the system displays perfectly synchronised magnetic oscillations in the long-time limit. This will occur for a wide range of specific parameters and initial states of the system, the only requirements are that the appropriate coefficients,  $D_i$ , are finite and the hopping amplitude  $\tau$  (which couples the different sites together) is non-zero. Moreover, in the thermodynamic limit, initial states which have  $\lim_{N \rightarrow \infty} \langle S^x \rangle / N \neq 0$  will ensure the long-time synchronised oscillations in  $\langle S_j^x \rangle$  have a finite amplitude [26]. Similarly to the previous example these oscillations are underpinned by long-range correlations in the system which arise due to the entangled nature of the long-time density matrix. We demonstrate these features in the following numerics, showing how the existence of a strong dynamical symmetry facilitates quantum synchronisation in a fully many-body quantum system.

In order to increase the system size accessible to our numerical calculations, we have used a ‘quantum trajectories’ approach [37] to perform a stochastic unravelling of Eq. (19) and simulate the dynamics at the level of an ensemble of pure wavefunctions. Furthermore in Fig. 7, as the simulation is only on a short time-scale, we were able to use the time-evolving block decimation [38] algorithm on a Matrix Product State [39] decomposition of the trajectory wavefunctions, further increasing the available system size. These simulations were performed with the aid of the Tensor Network Theory library [40].

In Fig. 7 we demonstrate the synchronicity which results from the eigenmodes in Eq. (20). We initialise the system in a product state and, after quenching under the Master Equation in Eq. (19) observe how the  $x$ -magnetisation on each site synchronises perfectly, oscillating at the anticipated frequency. The Pearson coefficient for the magnetisation on any two sites saturates to 1 in the long-time limit [Fig. 7(b)], with the dip at  $t\tau \approx 2$  being a transient effect which occurs at the first turning point in the magnetisation. Further figures, including the perfect distance-invariant oscillations of the two-point correlations, can be found in Ref. [26], where a possible experimental realisation of the system is also described.

We now perturb the system from the dynamical symmetry regime by setting the natural frequencies  $\omega_j$  to be inhomogeneous, here we draw them from an evenly spaced distribution, i.e.  $\omega_{j+1} - \omega_j = \text{const}$  and  $\omega_N - \omega_1 = 2\delta$ . Again, as for the spin-1 case, we choose this distribution for simplicity, our observations are independent of the explicit distribution - the key parameter is its width  $\delta$ . We initialise the system in a specified state and time-evolve under the Liouvillian in Eq. (19). In Fig. 8 we show how, similarly to the previous spin-1 example, the system is still attracted to the synchronised state, in both phase and frequency, on an intermediate time-scale. There is a significant band of detunings where the system stays in this long-lived synchronisation phase (Figs. 8a and b) and the spin on each site locks to the



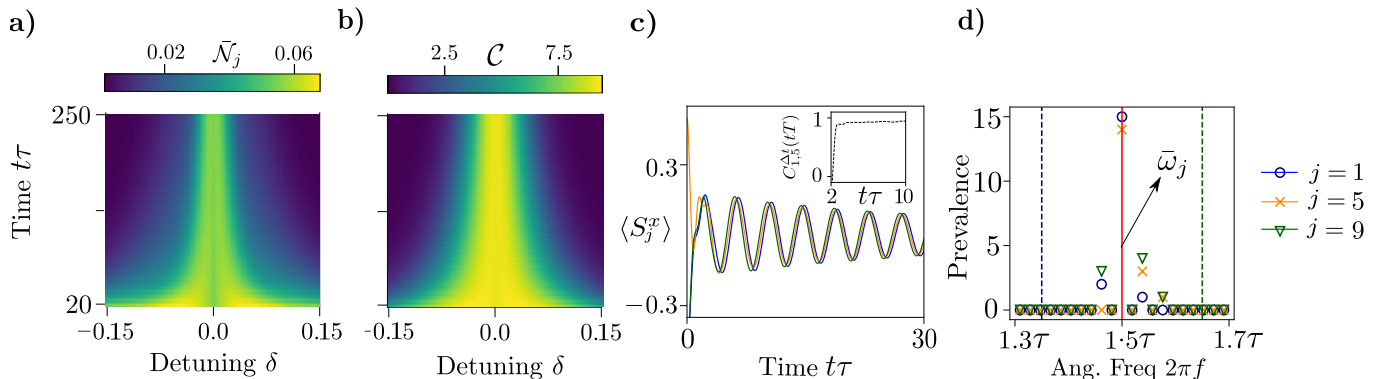


FIG. 8. a-b) Plot of synchronisation witnesses vs time and detuning for the charge-dephased Hubbard model with  $N = 5$  sites. The system is initialised in the state  $|\psi(0)\rangle = |\rightarrow\uparrow\rightarrow\uparrow\rangle$ , which has no double occupancies, where  $\rightarrow, \leftarrow, \uparrow$  and  $\downarrow$  correspond to each site being polarised in the positive  $x$ , negative  $x$ , positive  $z$  and negative  $z$  directions respectively. The system is then evolved in time with parameters  $\gamma = 2.0\tau, U = 0.5\tau$  and  $\mu_j \in \text{Rand}[0, 0.2]\tau$  where  $\text{Rand}[0, 0.2]$  is a uniformly-drawn random number on the specified interval. The magnetic frequencies are uniformly distributed  $\{\omega_1, \omega_2, \omega_3, \omega_4, \omega_5\} = \{1.0 - \delta, 1.0 - \delta/2, 1.0, 1.0 + \delta/2, 1.0 + \delta\}\tau$ . a) Synchronisation is measured by the average negativity for each site. b) Synchronisation is measured as the total magnitude of the off-diagonal coherences. (c) Example dynamics of  $\langle S_j^x \rangle$  for  $N = 9$ . The natural frequencies of the Hamiltonian are:  $\{\omega_1, \omega_2, \dots\} = \{1.35, 1.3875, \dots, 1.65\}\tau$  and other parameters are  $\gamma = 0.5\tau, U = 1.0\tau, \mu_j \in [0.0, 0.2]\tau$ . The starting state is  $|\psi(0)\rangle = \otimes_{j=1}^3 |\chi\rangle$  where  $|\chi\rangle = |\rightarrow\leftarrow\rightarrow\rangle$ . Inset) Pearson Coefficient for the two functions  $\langle S_1^x \rangle$  and  $\langle S_5^x \rangle$  over time with a rolling window of  $\Delta t = 2.0t\tau$ . d) Prevalence of different angular frequencies, extracted from the distribution of angular frequencies created using the time-periods between successive turning points for the oscillations in c) but up to  $t\tau = 90.0$ . Blue and green dashed lines indicate the expected delta function in the prevalence based on the natural frequency of spins 1 and 9. Red solid line indicates the average of all the natural frequencies  $\bar{\omega}_j$ . Only a subset of sites are represented in plots c-d) for clarity.

same phase and frequency (which is set by the average frequency of the individual sites, see Fig. 8d). Remarkably, this harmonized response is occurring even in the presence of both magnetic and chemical disorder - emphasizing the robustness of a symmetry-based approach to observing quantum synchronisation. The imaginary eigenmodes in Eq. (20) are translationally-invariant and hence  $\lambda^{(1)}$  evaluates to 0 (see Sec. IIC). As with the previous example, this robust, synchronised behaviour is a result of a second-order response to the detuning.

#### IV. CONCLUSION

We have shown how, using a combination of analytics and numerics, in generic open quantum systems the existence of a strong dynamical symmetry can facilitate the combination of entanglement and perfect phase synchronisation between the individual constituents. This is a direct result of the formation, in the long-time limit, of a well-defined phase relationship in the off-diagonal coherences of the density matrix, at all length-scales of the system. Furthermore, when perturbed from the dynamical symmetry regime these systems exhibit a second-order response which results in both phase and frequency locking throughout the system.

These observations originate at the level of the symmetries of the system. Thus, we believe, this work marks an important step in understanding how fully-quantum synchronisation can originate in a wide range of generic

physical systems - as opposed to in a single delicately controlled setup. We anticipate further examples of complex quantum networks where symmetry can guide the individual nodes into an entangled, fully synchronised state.

Finally, we highlight the potential role such a harmonised response can play in developing quantum technologies such as atomic clocks and other metrological instruments - which rely on quantum-enhanced synchronicity and cooperative behaviour in order to outperform their classical counterparts [41, 42].

#### ACKNOWLEDGMENTS

We would like to thank J. Mur-Petit and J. Coulthard for useful discussions. This work has been supported by EPSRC grants No. EP/P009565/1 and EP/K038311/1 and is partially funded by the European Research Council under the European Union's Seventh Framework Programme (FP7/2007-2013)/ERC Grant Agreement No. 319286 Q-MAC. In carrying out this work we acknowledge the use of the University of Oxford Advanced Research Computing (ARC) facility <http://dx.doi.org/10.5281/zenodo.22558>, the QuTiP Python toolbox for simulating open quantum systems <http://qutip.org> [43] and the Tensor Network Theory library [40] for performing the TEBD [38] algorithm which produced the data in Fig. 7.

- 
- [1] A. Pikovsky, M. Rosenblum, J. Kurths, and J. Kurths. *Synchronization: A Universal Concept in Nonlinear Sciences*. Cambridge Nonlinear Science Series. Cambridge University Press, 2003.
- [2] S. H. Strogatz and I. Stewart. Coupled oscillators and biological synchronization. *269(6)*:102–109, 1993.
- [3] L. M. Pecora, T. L. Carroll, G. A. Johnson, D. J. Mar, and J. F. Heagy. Fundamentals of synchronization in chaotic systems, concepts, and applications. *Chaos: An Interdisciplinary Journal of Nonlinear Science*, *7(4)*:520–543, Dec 1997.
- [4] Y. Kuramoto. Self-entrainment of a population of coupled non-linear oscillators. In *International Symposium on Mathematical Problems in Theoretical Physics*, pages 420–422, Berlin, Heidelberg, 1975. Springer Berlin Heidelberg.
- [5] S. H. Strogatz. From Kuramoto to Crawford: exploring the onset of synchronization in populations of coupled oscillators. *Physica D: Nonlinear Phenomena*, *143(1)*:1–20, 2000.
- [6] J. Buck. Synchronous rhythmic flashing of fireflies. ii. *The Quarterly Review of Biology*, *63(3)*:265–289, Sep 1988.
- [7] T. Vacharkulksemsuk and B. L. Fredrickson. Strangers in sync: Achieving embodied rapport through shared movements. *Journal of experimental social psychology*, *48(1)*:399–402, Jan 2012. 22389521[pmid].
- [8] J. P. Ramirez, L. A. Olvera, H. Nijmeijer, and J. Alvarez. The sympathy of two pendulum clocks: beyond Huygens’ observations. *Scientific Reports*, *6*:23580 EP –, Mar 2016. Article.
- [9] A. Roulet and C. Bruder. Synchronizing the smallest possible system. *Phys. Rev. Lett.*, *121*:053601, Jul 2018.
- [10] A. Roulet and C. Bruder. Quantum synchronization and entanglement generation. *Phys. Rev. Lett.*, *121*:063601, Aug 2018.
- [11] N. Jaseem, M. I. Hajdušek, V. Vedral, R. Fazio, L.-C. Kwek, and S. Vinjanampathy. Quantum Synchronisation in Nanoscale Heat Engines. *arXiv e-prints*, page arXiv:1812.10082, Dec 2018.
- [12] G.-j. Qiao, H.-x. Gao, H.-d. Liu, and X. X. Yi. Quantum synchronization of two mechanical oscillators in coupled optomechanical systems with Kerr nonlinearity. *Scientific Reports*, *8(1)*:15614, 2018.
- [13] T. E. Lee and H. R. Sadeghpour. Quantum synchronization of quantum Van der Pol oscillators with trapped ions. *Phys. Rev. Lett.*, *111*:234101, Dec 2013.
- [14] G. L. Giorgi, F. Galve, G. Manzano, P. Colet, and R. Zambrini. Quantum correlations and mutual synchronization. *Phys. Rev. A*, *85*:052101, May 2012.
- [15] G. Manzano, F. Galve, G. L. Giorgi, E. Hernández-García, and R. Zambrini. Synchronization, quantum correlations and entanglement in oscillator networks. *Scientific Reports*, *3(1)*:1439, 3 2013.
- [16] G. L. Giorgi, A. Cabot, and R. Zambrini. Transient synchronization in open quantum systems. *arXiv e-prints*, page arXiv:1907.06886, Jul 2019.
- [17] H. Ohadi, Y. d V-I. Redondo, A. J. Ramsay, Z. Hatzopoulos, T. C. H. Liew, P. R. Eastham, P. G. Savvidis, and J. J. Baumberg. Synchronization crossover of polariton condensates in weakly disordered lattices. *Phys. Rev. B*, *97*:195109, May 2018.
- [18] C. D. Tilley, C. K. Teoh, and A. D. Armour. Dynamics of many-body quantum synchronisation. *New Journal of Physics*, *20(11)*:113002, nov 2018.
- [19] S. Walter, A. Nunnenkamp, and C. Bruder. Quantum synchronization of two Van der Pol oscillators. *Annalen der Physik*, *527(1-2)*:131–138, Jan 2015.
- [20] T. E. Lee and H. R. Sadeghpour. Quantum synchronization of quantum van der Pol oscillators with trapped ions. *Phys. Rev. Lett.*, *111*:234101, Dec 2013.
- [21] C. D.-Tilley and A. D. Armour. Synchronization of micromasers. *Phys. Rev. A*, *94*:063819, Dec 2016.
- [22] S. Sonar, M. Hajdušek, M. Mukherjee, R. Fazio, V. Vedral, S. Vinjanampathy, and L. Kwek. Squeezing enhances quantum synchronization. *Phys. Rev. Lett.*, *120*:163601, Apr 2018.
- [23] N. Lörch, E. Amitai, A. Nunnenkamp, and C. Bruder. Genuine quantum signatures in synchronization of anharmonic self-oscillators. *Phys. Rev. Lett.*, *117*:073601, Aug 2016.
- [24] N. Lörch, S. E. Nigg, A. Nunnenkamp, R. P. Tiwari, and C. Bruder. Quantum synchronization blockade: Energy quantization hinders synchronization of identical oscillators. *Phys. Rev. Lett.*, *118*:243602, Jun 2017.
- [25] M. Ballerini, N. Cabibbo, R. Candelier, A. Cavagna, E. Cisbani, I. Giardina, A. Orlandi, G. Parisi, A. Procaccini, M. Viale, and V. Zdravkovic. Empirical investigation of starling flocks: a benchmark study in collective animal behaviour. *Animal Behaviour*, *76(1)*:201 – 215, 2008.
- [26] B. Buča, J. Tindall, and D. Jaksch. Non-stationary coherent quantum many-body dynamics through dissipation. *Nature Communications*, *10(1)*:1730, 2019.
- [27] O. Penrose and L. Onsager. Bose-Einstein Condensation and Liquid Helium. *Phys. Rev.*, *104*:576–584, Nov 1956.
- [28] C. N. Yang.  $\eta$  pairing and off-diagonal long-range order in a Hubbard model. *Phys. Rev. Lett.*, *63*:2144–2147, Nov 1989.
- [29] B. Buča and T. Prosen. A note on symmetry reductions of the Lindblad equation: transport in constrained open spin chains. *New Journal of Physics*, *14(7)*:073007, 2012.
- [30] D. A. Lidar, I. L. Chuang, and K. B. Whaley. Decoherence-free subspaces for quantum computation. *Phys. Rev. Lett.*, *81*:2594–2597, Sep 1998.
- [31] A. Beige, D. Braun, B. Tregenna, and P. L. Knight. Quantum computing using dissipation to remain in a decoherence-free subspace. *Phys. Rev. Lett.*, *85*:1762–1765, Aug 2000.
- [32] J. Tindall, B. Buča, J. R. Coulthard, and D. Jaksch. Heating-induced long-range  $\eta$  pairing in the Hubbard model. *Phys. Rev. Lett.*, *123*:030603, Jul 2019.
- [33] L.-H. Pan and C.-D. Gong. A note on Haldane’s conjecture. *Journal of Physics: Condensed Matter*, *20(21)*:215232, apr 2008.
- [34] F. Galve, G. L. Giorgi, and R. Zambrini. *Lectures on General Quantum Correlations and their Applications*, chapter Quantum Correlations and Synchronization Measures, pages 393–420. Springer International Publishing, Cham, 2017.
- [35] G. Vidal and R. F. Werner. Computable measure of entanglement. *Phys. Rev. A*, *65*:032314, Feb 2002.
- [36] F. H. L. Essler, H. Frahm, F. Göhmann, A. Klümper, and

- V. E. Korepin. *The One-Dimensional Hubbard Model*. Cambridge University Press, Cambridge, 2005.
- [37] A. J. Daley. Quantum trajectories and open many-body quantum systems. *Advances in Physics*, 63(2):77–149, Mar 2014.
  - [38] G. Vidal. Efficient classical simulation of slightly entangled quantum computations. *Phys. Rev. Lett.*, 91:147902, Oct 2003.
  - [39] F. Verstraete, V. Murg, and J.I. Cirac. Matrix product states, projected entangled pair states, and variational renormalization group methods for quantum spin systems. *Advances in Physics*, 57(2):143–224, 2008.
  - [40] S. Al-Assam, S. R. Clark, and D. Jaksch. The tensor network theory library. *Journal of Statistical Mechanics: Theory and Experiment*, 2017(9):093102, 2017.
  - [41] L. Pezzé and A. Smerzi. Entanglement, nonlinear dynamics, and the Heisenberg limit. *Phys. Rev. Lett.*, 102:100401, Mar 2009.
  - [42] R. Jozsa, D. S. Abrams, J. P. Dowling, and C. P. Williams. Quantum clock synchronization based on shared prior entanglement. *Phys. Rev. Lett.*, 85:2010–2013, Aug 2000.
  - [43] J. R. Johansson, P. D. Nation, and F. Nori. Qutip: An open-source python framework for the dynamics of open quantum systems. *Computer Physics Communications*, 183(8):1760–1772, 2012.

## V. SUPPLEMENTAL MATERIAL TO “QUANTUM SYNCHRONISATION ENABLED BY DYNAMICAL SYMMETRIES AND DISSIPATION”

### VI. PERTURBATION THEORY ON A FREQUENCY DETUNED LIOUVILLIAN

We consider a general Liouvillian formed from the Lindblad equation  $\mathcal{L}\rho = -i[H, \rho] + D[\rho]$ . The Hamiltonian contains, amongst other terms, an inhomogeneous field  $\sum_j \omega_j f_j$  where  $f_j$  is some local field operator. We can split the Hamiltonian into two terms, a homogeneous part:  $\sum_j \bar{\omega}_j f_j$  and an inhomogeneous part:  $\sum_j \delta_j f_j$  where  $\omega_j = \bar{\omega}_j + \delta_j$  and  $\bar{\omega}_j$  is the average natural frequency. We then, correspondingly, split the Liouvillian into a perturbed and an unperturbed part, scaling by  $1/\bar{\omega}_j$ :

$$\begin{aligned}\mathcal{L} &= \mathcal{L}^{(0)} + \epsilon \mathcal{L}^{(1)}, \quad \epsilon = \frac{\bar{\delta}_j}{\bar{\omega}_j}, \\ \mathcal{L}^{(0)} &= -\frac{i}{\bar{\omega}_j} [H - \sum_j \delta_j f_j, \bullet] + \frac{1}{\bar{\omega}_j} D[\bullet], \\ \mathcal{L}^{(1)} &= -i \left[ \sum_j \frac{\delta_j}{\bar{\omega}_j} f_j, \bullet \right],\end{aligned}\quad (22)$$

with  $\bar{\delta}_j$  is the average over the set of detunings  $\{\delta_j\}$ .

We work in superket and superbra form and assume that the unperturbed Liouvillian  $\mathcal{L}^{(0)}$  contains a series of imaginary eigenvectors and values  $\mathcal{L}^{(0)}|\rho_i^{(0)}\rangle = \lambda_i^{(0)}|\rho_i^{(0)}\rangle$ ,  $\text{Re}(\lambda_i^{(0)}) = 0$ , indexed by  $i$ . We let  $\langle\langle\sigma_i^{(0)}|$  denote the corresponding left-eigenvectors  $\langle\langle\sigma_i^{(0)}|\mathcal{L}^{(0)} = \lambda_i^{(0)}\langle\langle\sigma_i^{(0)}|$ . For small  $\epsilon \ll 1$  we expand the eigenvectors and values of the new Liouvillian  $\mathcal{L}$  as a perturbative power series on the previous, i.e.

$$\begin{aligned}|\rho_i\rangle &= |\rho_i^{(0)}\rangle + \epsilon|\rho_i^{(1)}\rangle + \epsilon^2|\rho_i^{(2)}\rangle + \dots, \\ \langle\langle\sigma_i| &= \langle\langle\sigma_i^{(0)}| + \epsilon\langle\langle\sigma_i^{(1)}| + \epsilon^2\langle\langle\sigma_i^{(2)}| + \dots, \\ \lambda_i &= \lambda_i^{(0)} + \epsilon\lambda_i^{(1)} + \epsilon^2\lambda_i^{(2)} + \dots\end{aligned}\quad (23)$$

We also know that the orthonormality condition  $\langle\langle\sigma_i|\rho_j\rangle\rangle = \text{Tr}(\sigma_i^\dagger \rho_j) = \delta_{i,j}$  must hold  $\forall \epsilon$  - where we have defined  $\sigma_i$  and  $\rho_j$  as the matrix forms of the corresponding superket and superbras. Using this condition, to 0th and 1st order, we have

$$\text{Tr} \left( \left( \sigma_i^{(0)} \right)^\dagger \rho_j^{(0)} \right) = \text{Tr} \left( \left( \sigma_i^{(1)} \right)^\dagger \rho_j^{(0)} + \left( \sigma_i^{(0)} \right)^\dagger \rho_j^{(1)} \right) = \delta_{ij}.\quad (24)$$

We now simplify the known expression  $\langle\langle\sigma_i|\mathcal{L}|\rho_i\rangle\rangle = \lambda_i\langle\langle\sigma_i|\rho_i\rangle\rangle$  by substituting the expansions in Eq. (24) and converting to matrix form. As a result we find the first order correction to the imaginary eigenvalue:

$$\lambda_i^{(1)} = \text{Tr} \left( \left( \sigma_i^{(0)} \right)^\dagger \mathcal{L}^{(1)} \rho_i^{(0)} \right).\quad (25)$$

For imaginary eigenmodes formed from a strong dynamical symmetry [26] it can be proved that the left and right eigenmodes are the same, i.e.  $\langle\langle\sigma_i^{(0)}| = \langle\langle\rho_i^{(0)}|$  and so

$$\begin{aligned}\lambda_i^{(1)} &= \text{Tr} \left( \left( \rho_i^{(0)} \right)^\dagger \mathcal{L}^{(1)} \rho_i^{(0)} \right) \\ &= -i \sum_j \frac{\delta_j}{\bar{\omega}_j} \text{Tr} \left( \left( \rho_i^{(0)} \right)^\dagger f_j \rho_i^{(0)} - \left( \rho_i^{(0)} \right)^\dagger \rho_i^{(0)} f_j \right).\end{aligned}\quad (26)$$

If the mode  $\rho_i^{(0)}$  is translationally invariant (i.e. it is unchanged under a permutation of any pair of sites) then we notice that the trace in Eq. (26) is independent of  $j$ . Using the fact  $\sum \delta_j = 0$  we have  $\lambda_i^{(1)} = 0$ : i.e for translationally-invariant imaginary eigenmodes formed from a strong dynamical symmetry we find that the system exhibits a non-linear response to perturbations in the homogeneity of the natural frequencies. This underpins the strong-synchronised response of the two systems considered in the main text.

### VII. IMAGINARY MODES AND STEADY STATES OF A SPIN 1 CHAIN

Here we prove the existence of certain imaginary modes and steady states of a dephased XXZ spin-1 chain of length  $N$ . In the main text, we consider the Lindblad equation

$$\begin{aligned}\frac{d\rho}{dt} = \mathcal{L}\rho &= -i[H, \rho] + \gamma \sum_{j=1}^N (S_j^z)^2 \rho (S_j^z)^2 - \frac{1}{2} \{ (S_j^z)^4, \rho \} \\ &= -i[H, \rho] + D[\rho],\end{aligned}\quad (27)$$

with the Hamiltonian  $H$

$$H = \omega \sum_{j=1}^N S_j^z + \sum_{j=1}^{N-1} J (S_j^+ S_{j+1}^- + S_j^- S_{j+1}^+) + \Delta S_j^z S_{j+1}^z.\quad (28)$$

We start by proving that any state  $\rho = \sum_{i=1}^{G_m} |m_i\rangle \langle m_i|$ , where  $|m_i\rangle$  is one of the  $G_m$  eigenvectors satisfying  $S_j^z |m_i\rangle = m |m_i\rangle$ , is a steady state:  $\mathcal{L}\rho = 0$ . Firstly we substitute  $\rho_{ss}$  into Eq. (27) where it is easy to show that  $[S_j^z, |m_i\rangle \langle m_i|] = [S_j^z S_{j+1}^z, |m_i\rangle \langle m_i|] = D[|m_i\rangle \langle m_i|] = 0$ ,  $\forall m, i, j$ . Hence, it remains to show

$$J \sum_{j=1}^{N-1} [S_j^+ S_{j+1}^- + S_j^- S_{j+1}^+, \sum_{i=1}^{G_m} |m_i\rangle \langle m_i|] = 0.\quad (29)$$

This can be done by considering the two spin-1s on the  $j$  and  $j+1$  positions for a given  $|m_i\rangle$ . Then, we have that  $S_j^+ S_{j+1}^- |m_i\rangle$  is a non-zero vector only if the two spin-1s are in one of the configurations  $|0 \uparrow\rangle, |00\rangle, |\downarrow \uparrow\rangle, |\downarrow \downarrow\rangle$ . Because, for these configurations, swapping spins  $j+1$

and  $j$  doesn't change the magnetisation  $m$  we can find always find the term  $|m_i\rangle\langle m_i|$  in the steady state, where  $|m_i\rangle$  is just  $|m_i\rangle$  with spins  $j$  and  $j+1$  swapped. Equation (29) then follows from the fact  $S_j^+ S_{j+1}^- |m_i\rangle\langle m_i| - |m_i\rangle\langle m_i| S_j^+ S_{j+1}^- = 0$ , i.e. for every term we can find a corresponding term to cancel it with.

We can also show that  $\mathcal{L} \sum_{i=1}^{G_m} |m_i\rangle\langle -m'_i| = 2im\omega \sum_{i=1}^{G_m} |m_i\rangle\langle -m'_i|$ , where  $\langle -m'_i|$  is the 'spin-flipped' bra for  $|m_i\rangle$  (i.e. if  $|2_1\rangle = |0\uparrow\uparrow\rangle$  then  $|-2'_1\rangle = |0\downarrow\downarrow\rangle$ ). Firstly, it is clear that  $[\sum_j S_j^z, |m_i\rangle\langle -m'_i|] = 2m |m_i\rangle\langle -m'_i|$ . Secondly, we also have  $[S_j^z S_{j+1}^z, |m_i\rangle\langle -m'_i|] = D[|m_i\rangle\langle -m'_i|] = 0 \forall m, i, j$ . Finally, by a very similar argument (the term with the  $j$  and  $j+1$  spins swapped can always be found in  $\sum_{i=1}^{G_m} |m_i\rangle\langle -m'_i|$ ) to the previous paragraph we find that  $\sum_{i=1}^{G_m} |m_i\rangle\langle -m'_i|$  satisfies Eq. (29) in the same manner as  $\sum_{i=1}^{G_m} |m_i\rangle\langle m_i|$ .

Hence we have another possible steady state:  $\mathcal{L} \sum_{i=1}^{G_0} |0_i\rangle\langle 0'_i| = 0$  and so we can write the full steady state as

$$\rho_{ss} = \sum_{m=-N}^N \left( \sum_{i=1}^{G_m} \lambda_m |m_i\rangle\langle m_i| \right) + \lambda'_0 \sum_{i=1}^{G_0} |0_i\rangle\langle 0'_i|, \quad (30)$$

which is  $2N+2$  fold degenerate. The coefficients  $\{\lambda_m\}$  and  $\lambda'_0$  must satisfy

$$\lambda'_0 + \sum_{m=-N}^N \lambda_m \sum_{s=0}^N \binom{N}{s} \binom{N-s}{(N-s+m)/2} = 1, \quad (31)$$

in order for  $\text{Tr}(\rho_{ss}) = 1$ . The terms in the second summation are skipped if  $(N-s+m)/2$  is not an integer.

Furthermore, the imaginary eigenmodes  $\rho_{1,0}^m = \sum_{i=1}^{G_m} |m_i\rangle\langle -m'_i|$   $m \neq 0, m = -N, \dots, N$ , which we proved satisfy  $\mathcal{L}\rho_{1,0}^m = 2im\omega\rho_{1,0}^m$ , originate as a series of strong dynamical symmetries [26] of the model because:

$$[H, \rho_{1,0}^m] = 2\omega m \rho_{1,0}^m, \quad [L_k, \rho_{1,0}^m] = [L_k^\dagger, \rho_{1,0}^m] = 0 \quad \forall k, m. \quad (32)$$

I.e. for this system the strong dynamical symmetry operators are the imaginary modes because they return themselves upon application to the steady state  $\rho_{1,0}^m \rho_{ss} \propto \rho_{1,0}^m$  (the steady state is singular). Further application of the strong dynamical symmetry operators is redundant as  $\rho_{1,0}^m \rho_{1,0}^m = 0$ . For the case when  $N > 2$  and  $\Delta \neq 0$  numerical calculations show that these  $2N+2$  steady states and  $2N$  imaginary modes completely span the kernel of  $\mathcal{L}$  and thus form a complete description of the system's dynamics in the limit  $t \rightarrow \infty$ .

## VIII. LONG-TIME DYNAMICS OF THE SPIN 1 CHAIN

As the imaginary modes  $\rho_{1,0}^m$  contain coherences between the states  $|\uparrow\rangle$  and  $|\downarrow\rangle$  then they will only affect

the dynamics of quadratic observables such as  $(S_j^x)^2$  and  $(S_j^y)^2$ . We can always write the long-time density matrix as:

$$\lim_{t \rightarrow \infty} \rho(t) = C_0 \rho_{ss} + \left( \left( \sum_{m=1}^N e^{2i\omega m t} C_m \rho_{1,0}^m \right) + \text{h.c.} \right) \quad (33)$$

where  $C_m$  are a series of real coefficients (to ensure hermiticity) associated with the overlap between the initial state  $\rho(t=0)$  and either the steady state  $\rho_{ss}$  or the imaginary modes  $\rho_{1,0}^m$ . We also have  $(\rho_{1,0}^m)^\dagger = \rho_{1,0}^{-m}$ . We consider the expectation value of the operator  $(S_j^x)^2 = (1/4)(S_j^+ + S_j^-)^2$ . As the imaginary modes for which  $|m| \geq 2$  must contain at least two flipped spins between the states  $|m_i\rangle$  and  $\langle -m_i|$  then we immediately have  $\text{Tr}(\rho_{1,0}^m (S_j^x)^2) = 0$ ,  $|m| \geq 2 \forall j$ . Hence, we get:

$$\begin{aligned} \lim_{t \rightarrow \infty} \langle (S_j^x)^2 \rangle(t) \\ = C_0 \text{Tr}(\rho_{ss} (S_j^x)^2) + 2C_1 \cos(2\omega t) \text{Tr}(\rho_1 (S_j^x)^2), \end{aligned} \quad (34)$$

where we have used the fact  $\text{Tr}(\rho_{-1} (S_j^x)^2) = \text{Tr}(\rho_1 (S_j^x)^2)$ . Equation (34) proves the formation of clean, single frequency oscillations in the associated observable. Furthermore, the modes  $\rho_{ss}$  and  $\rho_{1,0}^m$  are all translationally invariant and so the oscillations are identical for all spins: ensuring perfect phase synchronisation.

In order to observe the excitement of higher order modes we must measure higher order correlators. Specifically consider the operator

$$X = \prod_{j \in \{a,b,c,\dots\}} (S_j^x)^2, \quad |\{a,b,c,\dots\}| = M \quad (35)$$

where the set of  $M$  sites  $\{a,b,c,\dots\}$  contains no duplicates. Because we now have  $\text{Tr}(\rho_{1,0}^m X) \neq 0$ ,  $m \leq M$  and  $\text{Tr}(\rho_{1,0}^m X) = \text{Tr}(\rho_{1,0}^{-m} X)$  then we find

$$\langle X \rangle = C_0 \text{Tr}(\rho_{ss} X) + 2 \sum_{m=1}^M C_m \cos(2m\omega t) \text{Tr}(\rho_{1,0}^m X), \quad (36)$$

and see the appearance of higher order frequencies due to the excitement of higher order imaginary modes. This explains the Fourier Spectrum observed in Fig. 4b) in the main text.

## IX. PARAMETRISING THE CROSS-SECTIONS OF THE FREQUENCY-DETUNED SPIN-1 CHAIN

In the main text we considered the response of the system when the magnetic field is inhomogeneous, i.e. the system's dynamics is modelled by Eq. (27) with the



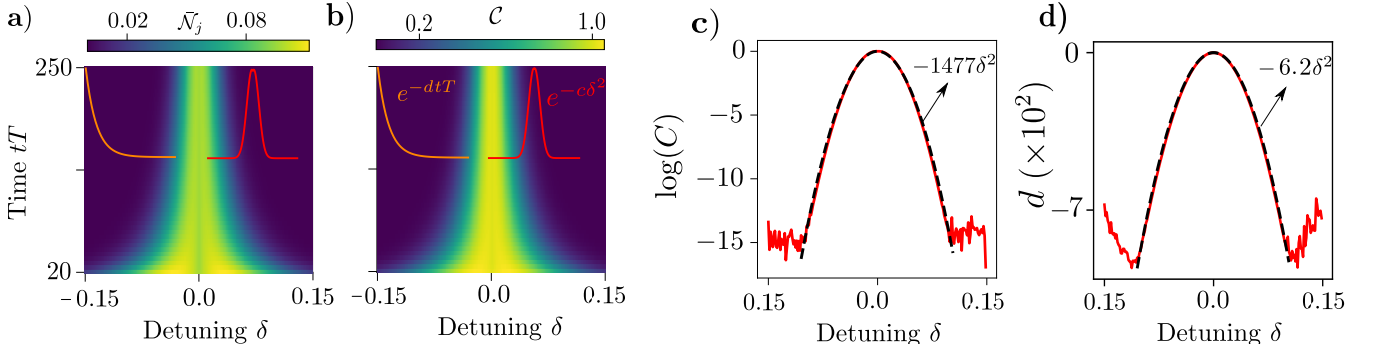


FIG. 9. a-b) Reproduced from main text, plot of synchronisation witnesses vs time and detuning for the dephased spin-1 chain described by Eq. (27) and with  $N = 3$ . The system is initialised in the state  $|\psi(0)\rangle = |\rightarrow 00\rangle$ , where  $|\rightarrow\rangle = \frac{1}{\sqrt{2}}(|\uparrow\rangle + |\downarrow\rangle)$ , and evolved in time with parameters  $\{\omega_1, \omega_2, \omega_3\} = \{1.0 - \delta, 1.0, 1.0 + \delta\}J$ ,  $\gamma = 2.0J$ ,  $\Delta = 0.5J$ . Insets, top-left) Cross-section (orange) of these measures versus time at detuning  $\delta = -0.075$ . top-right) Cross-section (orange) of these measures versus detuning at time  $tJ = 250.0$ . The parameters  $d$  and  $c$  are used to parametrise the cross-sections. a) Synchronisation is measured by the average negativity for each site. b) Synchronisation is measured as the total magnitude of the off-diagonal coherences. c) Natural logarithm of the off-diagonal coherences  $C$  versus the detuning, taken from the inset in the top right of b). Dotted line is a quadratic fit over  $\delta \in [-0.1, 0.1]$  d) Decay coefficient  $d$  (fitted to the exponential decay of  $C$  versus time  $tJ$ ) versus detuning. Dotted line is a quadratic fit over  $\delta \in [-0.1, 0.1]$ .

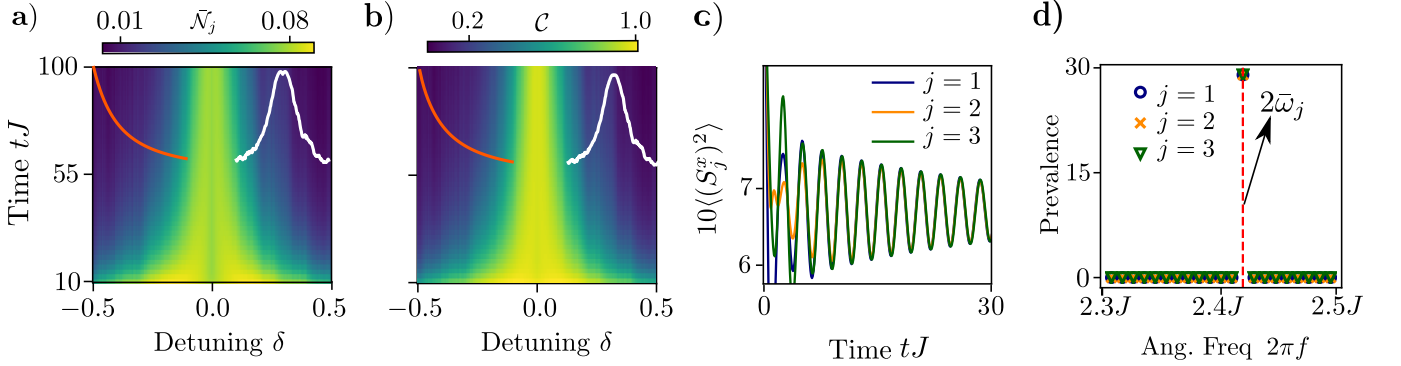


FIG. 10. a-b) Plot of synchronisation witnesses vs time and detuning for Eq. (27). The system is initialised in the state  $|\psi(0)\rangle = |\rightarrow 00\rangle$  and evolved in time with parameters  $\omega_j = (1 + \epsilon_j)J$ ,  $\gamma = 2.0J$ ,  $\Delta = 0.5J$  and random detuning  $\epsilon_j \in [0, \delta]$  where  $[0, \delta]$  is a uniform random distribution over the specified interval. The Synchronisation measures are then averaged over 100 instances of disorder associated with the detuning. Insets) top-left, orange, shows the witness versus time at detuning  $\delta = -0.25$ . Top-right, white, shows the witness versus detuning at time  $tJ = 55.0$ . a) Synchronisation is measured by the average negativity,  $\bar{N}_j$ , for each site. b) Synchronisation is measured as the total magnitude of the off-diagonal coherences  $\bar{C}$ . c) Example dynamics of  $\langle (S_j^x)^2 \rangle$  for the same system except with specific natural frequencies  $\{\omega_1, \omega_2, \omega_3\} = \{1.258, 1.210, 1.160\}J$  (drawn from a uniform random distribution). d) Prevalence of angular frequencies, extracted from the distribution of angular frequencies created using the time-periods between successive turning points for the oscillations in c) but up to  $tJ = 100.0$ . The central line is twice the average of the spin's natural frequencies  $\bar{\omega}_j$ .

Hamiltonian now of the form

$$H = \sum_{j=1}^N \omega_j S_j^z + \sum_{j=1}^{N-1} J(S_j^+ S_{j+1}^- + S_j^- S_{j+1}^+) + \Delta S_j^z S_{j+1}^z. \quad (37)$$

where the  $\omega_j$  are a series of natural frequencies associated with each spin  $j$ . We then considered how, for a given range of natural frequencies, synchronisation witnesses such as the negativity  $\mathcal{N}_j(\rho) = \frac{\|\rho^{T_j}\| - 1}{2}$  [35] or off-diagonal coherences  $\mathcal{C} = \sum_{i \neq j} |\rho_{ij}|$  [11] evolve in time. For the example in the main text we considered  $N = 3$  with the natural frequencies equally spaced

$\{\omega_1, \omega_2, \omega_3\} = \{1 - \delta, 1, 1 + \delta\}J$ , which produced the maps in Fig. 9(a-b), showing the witnesses as a function of time and detuning.

We now parametrise the cross-sections in Fig. 9(b). In Fig. 9(c) we show how, at a given time, and for sufficiently small detunings, the off-diagonal coherences  $C$  are well-described by a Gaussian curve as a function of the detuning. Furthermore, in Fig. 9(d) we calculate the decay coefficient (for the exponential decay of the off-diagonal coherences  $C$  versus time) versus  $\delta$ , showing how, for small detunings,  $d \propto \delta^2$ . In Figs. 9(c-d) the tails of the distribution aren't captured by this parametrisation due to

numerical precision (both synchronisation quantities are very close to 0 for large detunings). This parametrisation also holds for the cross-sections of the average negativity  $\bar{N}_j$  in Fig. 9(b).

## X. FURTHER PLOTS OF THE FREQUENCY-DETUNED SPIN-1 CHAIN

In Figure 5 of the main text we showed how, when the natural frequencies of the spins in the chain are inhomogeneous, the system still locks to a long-lived, synchronised cycle with a frequency which is the average of their natural frequencies. This response emerges as a tongue-like profile in the witnesses  $\mathcal{C}$  and  $\bar{N}_j$  as a function of detuning  $\delta$  and time. In the main text, for simplicity, we considered the case where  $\{\omega_1, \omega_2, \omega_3\} = \{1.0 - \delta, 1.0, 1.0 + \delta\}$ , i.e. the natural frequencies form a uniform sequence. Here, in Fig. 10, we show that this distribution is arbitrary, showing how similar tongues and cross-sections emerge when the natural frequencies are drawn from a uniform random distribution of width  $\delta$ . The spins are able to lock to an intermediate cycle with a frequency which is twice the average of the natural frequencies  $\bar{\omega}_j$ .

## XI. PERSISTENT LIMIT CYCLES OF THE CHARGE-DEPHASED HUBBARD MODEL

Now, we turn our attention to the Hubbard model. The Lindblad equation in this case reads

$$\begin{aligned} \frac{\partial \rho}{\partial t} &= \mathcal{L}\rho = -i[H, \rho] + \gamma \sum_{j=1}^N S_j^z \rho S_j^z - \frac{1}{2} \{S_j^z, \rho\} \\ &= -i[H, \rho] + D[\rho], \end{aligned} \quad (38)$$

with the Hamiltonian  $H$

$$\begin{aligned} H &= -\tau \sum_{\langle jl \rangle, \sigma} (c_{\sigma, j}^\dagger c_{\sigma, l} + \text{h.c.}) + \sum_j U n_{\uparrow, j} n_{\downarrow, j} + \omega \sum_j S_j^z, \\ S_j^z &= n_{\uparrow, j} - n_{\downarrow, j}. \end{aligned} \quad (39)$$

It is known [26] that the imaginary eigenmodes of this Liouvillian are:

$$\begin{aligned} \rho_{nm} &= (A)^n \rho_{ss} (A^\dagger)^m, \quad \mathcal{L}\rho_{nm} = i(m-n)\omega \rho_{nm}, \\ A &= S^+ = \sum_j c_{j, \uparrow}^\dagger c_{j, \downarrow} \end{aligned} \quad (40)$$

where  $\rho_{ss}$  is a grand-canonical-like state containing the strong-symmetries of the system [26, 29, 32] and  $\rho_{n, m}^\dagger = \rho_{m, n}$ . Thus in the long-time limit the state of the system can be written as

$$\lim_{t \rightarrow \infty} \rho(t) = \sum_{\substack{n, m \\ n \geq m}} C_{n, m} e^{i(m-n)\omega t} \rho_{n, m} + \text{h.c.}, \quad (41)$$

where the  $C_{n, m}$  are a series of real coefficients associated with the overlap between the initial state and the modes  $\rho_{n, m}$ . We calculate the expectation value of the operator  $S_j^x$

$$\lim_{t \rightarrow \infty} \langle S_j^x \rangle(t) = \sum_{\substack{n, m \\ n \geq m}} C_{n, m} e^{i(m-n)\omega t} \text{Tr}(S_j^x \rho_{n, m}) + \text{h.c.} \quad (42)$$

By expressing  $S_j^x$  in terms of raising and lowering operators and using the fact that a)  $\text{Tr}(S_j^x \rho_{n, m}) = \text{Tr}(S_j^x \rho_{m, n})$  and b) the trace vanishes unless  $|m - n| = 1$  (as the operator  $S_j^x \rho_{n, m}$  will have no diagonal elements in the eigenbasis of  $\rho_{ss}$ ) we get

$$\lim_{t \rightarrow \infty} \langle S_j^x \rangle(t) = 2 \cos(\omega t) \sum_{n=1} C_{n, n-1} Y_{n, n-1}, \quad (43)$$

with  $Y_{n, n-1} = \text{Tr}(S_j^x \rho_{n, n-1}) = \text{Tr}(S_j^x \rho_{n-1, n})$ . Hence, we see persistent oscillations in  $S_j^x$ , which are centred around the  $x$ -axis. The modes  $\rho_{n, m}$  are completely translationally invariant and thus the spins on each site will synchronise to limit cycles perfectly in phase, regardless of the initial state. We can immediately treat higher order modes through the operator

$$X = \prod_{j \in \{a, b, \dots\}} S_j^x, \quad |\{a, b, \dots\}| = M, \quad (44)$$

where the set of  $M$  sites  $\{a, b, c, \dots\}$  contains no duplicates. We can calculate the expectation value of this operator by expanding it in terms of raising and lowering operators and using the fact the trace of each term is only non-vanishing if the difference between the number of raising and lowering operators is equal to  $|m - n|$ . Thus, we get

$$\lim_{t \rightarrow \infty} \langle X \rangle(t) = \sum_{i=0}^{\lfloor M/2 \rfloor} D_i \cos((2i + d)\omega t), \quad d = M \bmod 2, \quad (45)$$

where the  $D_i$ 's are a series of coefficients based on the initial state and the various traces between the  $\rho_{n, m}$ s and products of local spin-raising and lowering operators.